Front. Optoelectron. China 2011, 4(2): 130–136
DOI 10.1007/s12200-011-0168-3

RESEARCH ARTICLE

Substrate effect on morphology and photoluminescence from ZnO monopods and bipods

Pijus Kanti SAMANTA (✉)[1], Partha Roy CHAUDHURI[2]

1 Department of Physics, Rabindra Satabarsiki Mahavidyalaya, Ghatal-721212, West Bengal, India
2 Department of Physics & Meteorology, Indian Institute of Technology Kharagpur, West Bengal, India

© Higher Education Press and Springer-Verlag Berlin Heidelberg 2011

Abstract A simple wet chemical bath deposition has been successfully deployed to fabricate zinc oxide (ZnO) nanostructures. For substrate free growth, the nanostructure is spindle like monopods. But when the nanostructures grow on the glass and quartz substrates, they are bipods (two monopods joined together base to base). Variation in the size of the spindles of the monopods and bipods and the particle size was observed due to the strain exists in the thin film due to lattice mismatch at the interface of the thin film and the substrates. The X-ray diffraction (XRD) and selected area diffraction results confirmed the hexagonal unit cell structures of the monopods and bipods. Also the growth rates of various planes are different and the growth is anisotropic. The substrate free grown monopods show visible photoluminescence (PL) at 421 nm. But the emission gets shifted by 3 and 6 nm for ZnO thin film deposited on quartz and glass substrates respectively due to interfacial strain. In case of ZnO on quartz substrate a strong ultra-violet (UV) peak was observed at 386 nm due to band edge transition. These emissions are also accompanied by few weaker emission peaks due to various defect related transition.

Keywords monopods, bipods, particle-size, strain, photoluminescence (PL), recombination

1 Introduction

Zinc oxide (ZnO) nanostructures, especially nanorods, nanotubes, nanoparticles, are of immense interests since the last few years due to their versatile properties like near ultra-violet (UV) [1] and visible (green [2], blue [3] and violet [4]) emission, electrical conductivity [5], optical transparency [6], and piezoelectricity [7] and many other promising applications in gas sensors, photovoltaic devices and optical solar cells [8] and optoelectronic devices. Due to its wide band gap of 3.37 eV at room temperature and a huge exciton binding energy of 60 meV, it is being extensively investigated towards its short wavelength light emitting, and room temperature ultraviolet lasing [9] applications. Varieties of ZnO nanostructures so far have been fabricated and their photoluminescence (PL) have also been studied by many researchers. The UV emission that originates due to the band edge transition or the exciton transition is the characteristic emission for zinc oxide. But visible emissions are also reported that occurs from different defect states (several oxygen vacancies, Zn interstitials, etc.) of ZnO [10–12]. These emissions from ZnO depend on the shape and size of the fabricated nanostructures. Hence control over the shape, size and the existence of different defect states in the nanostructures (during synthesis process) play an important role towards the technological implementations in different luminescent and nanophotonic devices.

Due to device-based applications there is an inherent interest to grow various ZnO nanostructures on different substrates like glass, quartz, Si, Zn-foil, etc. However interesting structural modifications were observed while growing the nanostructures on various substrates. Besides, substrates affect the luminescence behaviour of the material. Teng et al. had reported the PL in the UV region at ~380 nm (UV-PL) from ZnO thin film grown on Si substrate [13]. This emission peak shifts to 395 nm for the sample grown on ITO/Si substrate. This UV-PL occurs due to band edge transition whereas the 395 nm peak appeared due to the recombination located between ZnO and ITO substrates. In this context, varieties of ZnO nanostructures have been fabricated by different fabrication processes like physical and chemical vapour deposition [14], hydrothermal process [15], vapour-liquid-solid method [16], electrochemical deposition [17] and laser ablation [18].

Received November 15, 2010; accepted November 30, 2010

E-mail: pijush.samanta@gmail.com

But most of these processes are constrained to maintenance of rigorous experimental conditions and involved with many complicated steps and they need huge infrastructures.

In this paper, we outline a simple chemical route towards the repeated synthesis of ZnO monopods and bipods followed by a few typical characterization results with a view to study the influence of substrate on the morphology and PL from ZnO nanostructures. This is a very simple table-top experiment quite suitable to adopt in laboratory environment and easily repeatable. In this method we have been able to synthesize spindle like ZnO nanostructures on different substrates which shows strong PL in the UV region of wavelength which is the characteristic emission of ZnO. Those emissions are accompanied by visible emission peaks due to various defects related transition. We discuss, in detail, the effect of substrate on the morphology of the nanostructures and also the mechanism of various PL peaks.

2 Experiment and characterizations

All reagents used were of analytical grade (Merck) and need no further purification. In our typical synthesis process zinc nitrate solution (0.5 M) was prepared by dissolving 14.87 g $Zn(NO_3)_2$ in water to prepare 100 mL solution. NaOH (1 M) solution was prepared by dissolving 4 g NaOH in water to prepare 100 mL solution. Under constant stirring of NaOH solution the above zinc nitrate solution was added drop wise for 15 min. After 30 min constant stirring the solution was heated so that it started boiling. Now different substrates (glass, quartz) were dipped in the solution by a simple clamp stand arrangement. The boiling was continued to 45 min. After cooling the solution to room temperature, the substrates were taken out of the solution. A white film was deposited on the substrates. The substrates were then cleaned several times by distilled water and dried at 50°C for further characterizations. A white precipitate was also collected from the bottom. The powder is then dried in an ordinary oven for further characterizations.

Grazing incidence X-ray diffraction (GIXRD) data were collected (for thin films) using Phillips X'Pert PRO X-ray diffractometer in the angular range of $30° < 2\theta < 60°$ with Cu-Kα radiation of wavelength 1.54 Å. For the precipitated powder sample X-ray diffraction (XRD) was carried out in an ordinary Rigaku diffractometer that used Cu-Kα as X-ray source and scanned over an angular range $30° < 2\theta < 60°$. The morphology of the structures was studied using Zeiss field emission scanning electron microscope (FESEM). The room temperature photoluminescence spectra were recorded using PerkinElmer LS-55 spectrophotometer with an Xenon lamp at the excitation of 325 nm.

3 Results and discussion

3.1 X-ray diffraction (XRD)

Figures 1–3 show the XRD pattern of the ZnO nanostructures grown without any substrate (monopods) and grown on different glass and quartz substrates respectively. The patterns are indexed with hexagonal unit-cell structure which is consistent with the JCPDS card no-36-1451. We also observe in Fig. 3 that in the case of quartz a peak of very high intensity was observed at 46.7° that arises due to the quartz substrate itself. The ratio of intensities of the various diffraction peaks is different in different cases. It indicates that the growth rate of various planes of ZnO grown on different substrates is different. The growth rate of different planes for glass and quartz substrate is $V(101) > V(100) > V(002) > V(110) > V(102)$. But in absence of substrate the growth rate of various plane is somewhat different and is $V(101) > V(100) > V(002) > V(102) > V(110)$. This is because of the fact that in presence of the substrate the growth rate is modified due to strain at the ZnO thin film and substrate interface.

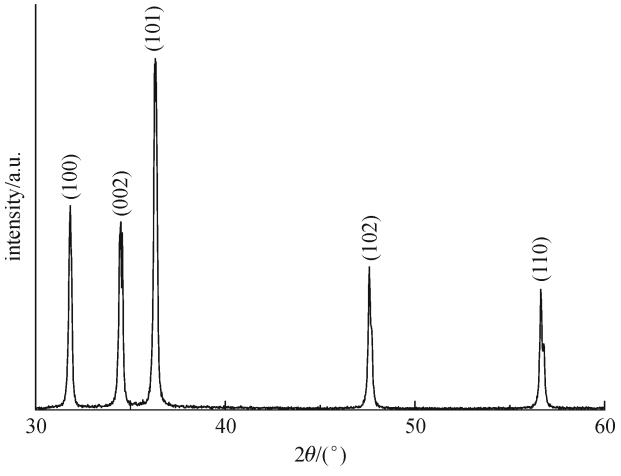

Fig. 1 XRD pattern of ZnO monopods grown without any substrate

Particle sizes and strain were calculated from the XRD pattern using Scherer formula [19]:

$$t = \frac{K\lambda}{\Delta(2\theta)\cos\theta} \quad \text{and} \quad \varepsilon = \frac{\beta}{4\tan\theta}, \tag{1}$$

where λ is the wavelength of X-ray used, $K = 0.89$, θ is the angle of diffraction, and $\Delta(2\theta)$ is the full-line width at half maxima (FWHM). The particle size of the ZnO bipods is found to be 35 nm for glass, 33 nm for quartz. However the particle size of the monopods was found to be 38 nm. In all the cases there was no significant difference in the particle size for different substrates as shown in Table 1. The strain is more for the quartz substrate as compared to glass and

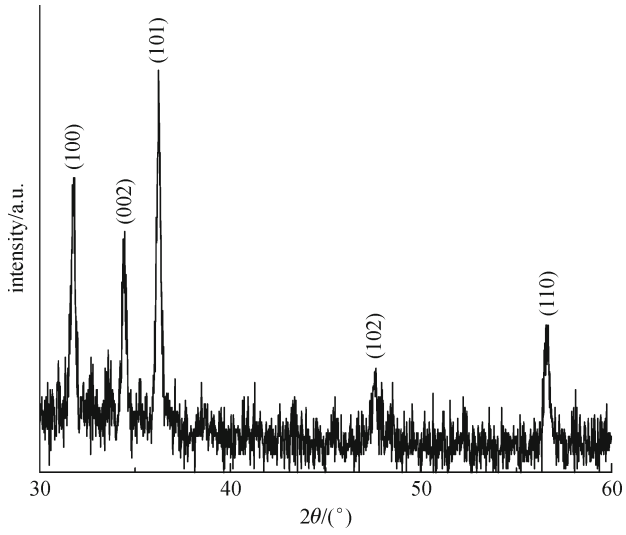

Fig. 2 XRD pattern of ZnO bipods grown on glass

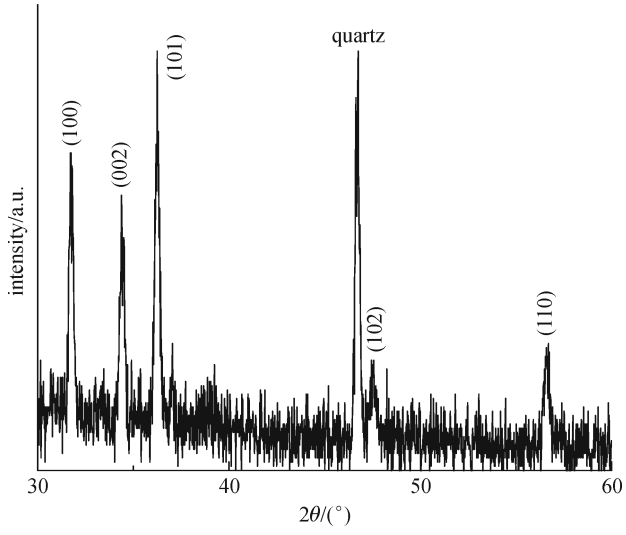

Fig. 3 XRD pattern of ZnO monopods grown on quartz

Table 1 Data for particle size and strain for different substrates

substrates	FWHM	2θ/(°)	particle size/nm	strain
no substrate	0.21695	36.31	38	0.1654
glass	0.23202	36.23	35	0.1773
quartz	0.24605	36.25	33	0.1868

hence the particle size is less for ZnO grown on quartz substrate. The variation of strain with particle size is shown in Fig. 4.

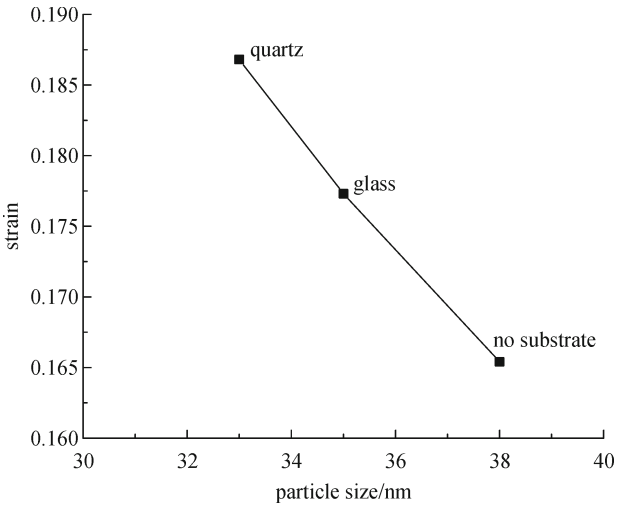

Fig. 4 Variation of strain with particle size

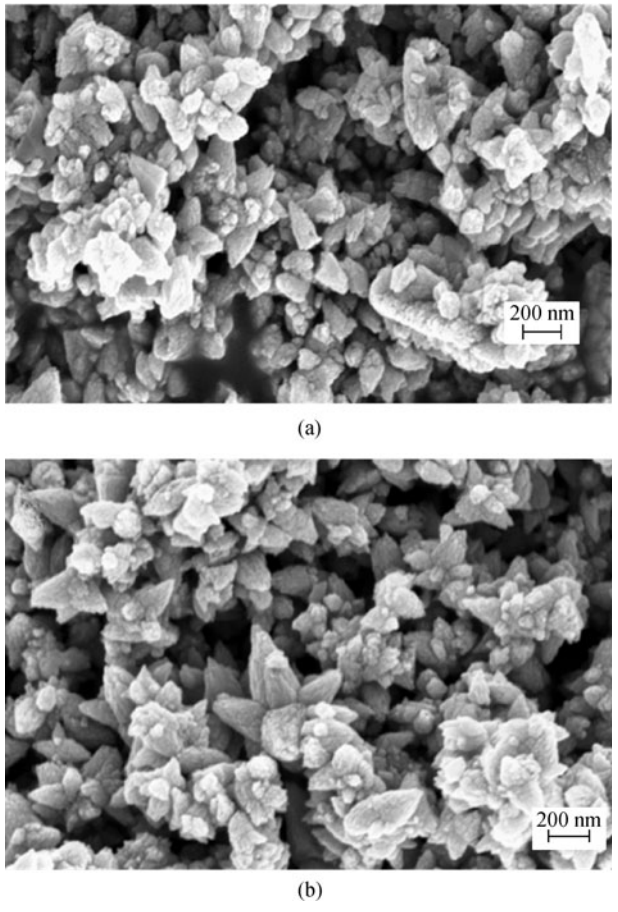

Fig. 5 FESEM images of prism-like monopods grown without any substrate taken in two different positions

3.2 Field emission scanning electron microscopy (FESEM)

Figures 5(a) and 5(b) show the FESEM images of prism-like monopods as observed in the case of the precipitated powder samples. Zinc nitrate on reaction with NaOH produces ZnO nanorods at room temperature [20]. On increasing reaction temperature up to the boiling of the solution the rods are transformed into prism-like

monopods. But in the same reaction process while different substrates were dipped in the solution, a thin film was deposited, in which the particles are like bipods, two monopods joined together base to base (Fig. 6). The particles are distributed in the thin film which is evident from the FESEM images. The monopods and bipods are ~100–150 nm in length and the waist size is about 80–100 nm. No preferential growth was observed for these structures. So in the present case the morphology of the nanostructures strongly depends on the substrates. It should be mentioned that in case of substrate assisted growth of the nanostructures, the bipods-like structures consist of two monopods which are almost half the size of the monopods observed in case of substrate free growth. Thus we conclude that the nanostructures are much more strained while grown on the substrate.

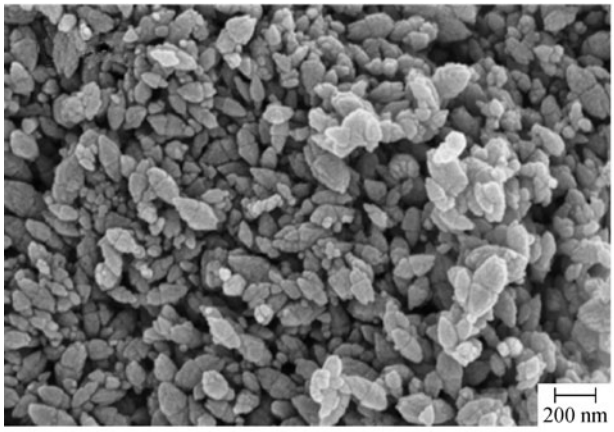

Fig. 6 FESEM images of bipods grown on (a) glass and (b) quartz substrate

3.3 Growth mechanism

ZnO exhibit hexagonal closed packed structure with Zn atoms in tetrahedral position as shown in Fig. 7. It belongs to the space group $P_6 3mc$. There is no centre of inversion

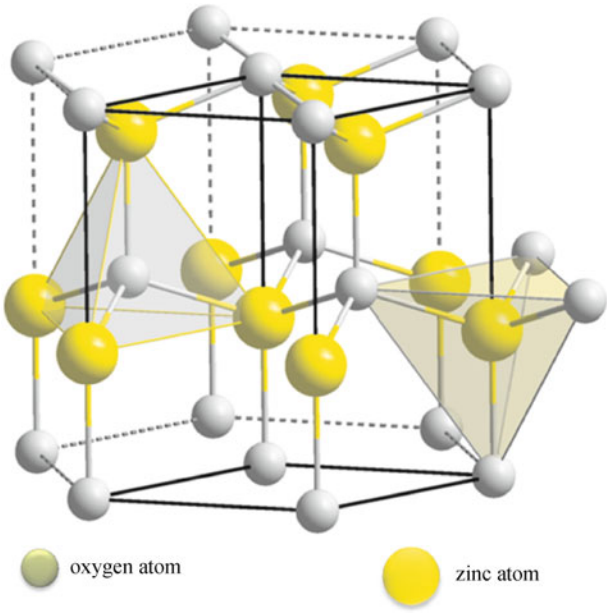

Fig. 7 Hexagonal crystal structure of ZnO

in wurtzite structure. Hence there exists an inherent asymmetry along the *c*-axis of the crystal. Thus in chemical synthesis of ZnO nanostructures anisotropic growth along (0001) direction is observed. ZnO crystal has the maximum growth rate along (0001) direction; hence the hexagonal crystal structure of ZnO is related to the relative growth rate of different crystal facets [20].

In a typical aqueous solution-based growth, $Zn(NO_3)_2$ solution, on reaction with NaOH, produces $Zn(OH)_2$ which continues further to form $Zn(OH)_4^{2-}$. At the onset of supersaturation ZnO nuclei will form. These ZnO nuclei are small and rod-like structures. On increasing the reaction temperature they are transformed to prism-like structures (see Fig. 5). While using the substrate, the prisms are then linked together to form polycrystalline bipods (see Fig. 6). In the solution growth process $Zn(OH)_4^{2-}$ nuclei serves as the nucleation centre for the growth of rod-like ZnO nanostructures and growth rate of different crystal planes in a simple hydrothermal process [21] is $V(0001) > V(01\bar{1}\bar{1}) > V(01\bar{1}0) > V(01\bar{1}1) > V(000\bar{1})$. Now due to the rapid growth rate of the (0001) plane it will be disappeared quickly. Thus this plane disappears in the experimentally synthesized ZnO nanocrystals leading to the rod-like structure. When the reaction temperature is increased (about 900°C), due to heat convection and deregulation movements of the molecules and ions, deposition of $Zn(OH)_4^{2-}$ will be very fast. Now according to the above growth process $(01\bar{1}0)$ plane may grow faster than $(01\bar{1}1)$ plane. So $(01\bar{1}0)$ plane extrudes. As a result the prisms like ellipsoidal nanocrystals are formed [22]. Now these prisms like nanocrystals are joined together via the oriented attachment end to end along the

major axis and side by side along semi minor axis. As a result the ellipsoidal bipods like structures were observed. However the growth of these types of nanostructures needs further investigations. A schematic of the growth of the bipods is shown in Fig. 8.

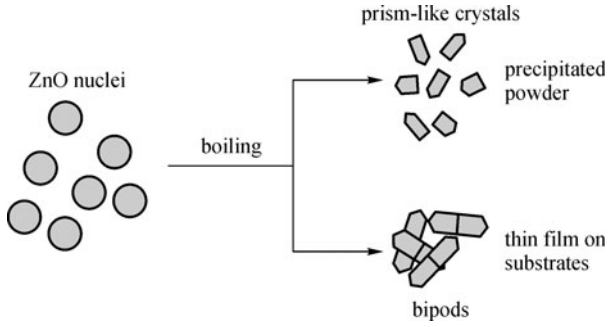

Fig. 8 Schematic of growth of monopods and bipods

3.4 Transmission electron microscopy (TEM)

Transmission electron microscopic was also carried out for further structural study of the fabricated nanostructures. Figures 9(a) and 9(b) show TEM images of the nanobipods grown over the glass substrate. The spindles are about 100–150 nm in length and the waist diameter is about 80–100 nm. The bipods are actually consisting of two prisms joined base to base which can be clearly observed from Figs. 9(a) and 9(b). The selected area diffraction pattern reveals that the prisms are polycrystalline (see Fig. 9(c)).

3.5 Photoluminescence (PL)

PL spectra were carried out to study the optical emission property of the thin films. Figure 10 shows the PL spectra of the thin film grown on different substrates. UV emission is the characteristic emission of ZnO. This emission occurs due to band edge transition. However visible emission is also reported by many researchers in the recent years [2–8]. Nanocrystals or quantum dots, produced by chemical methods, normally have more defects, lattice distortion, crystal-imperfection, vacancies, stacking faults, grain boundaries and dislocations compared to the bulk crystals. These defects produce shallow deep levels of lower energy. These deep levels are responsible for various visible emission peaks in the PL spectrum of nanocrystalline ZnO. Vanheusden et al. [2] had reported that the visible luminescence of ZnO mainly originates from different defect states such as oxygen vacancies and Zn interstitials. Oxygen, in general, exhibit three types of charge states of oxygen vacancies such as V_o^0, V_o^+, and V_o^{2+}. The oxygen vacancies are located below the bottom of the conduction band (CB) in the sequence of V_o^0, V_o^+, and V_o^{2+}, from top to bottom. Interstitial Zn also plays a major role in lattice distortion in the nanocrystals. Due to high surface to

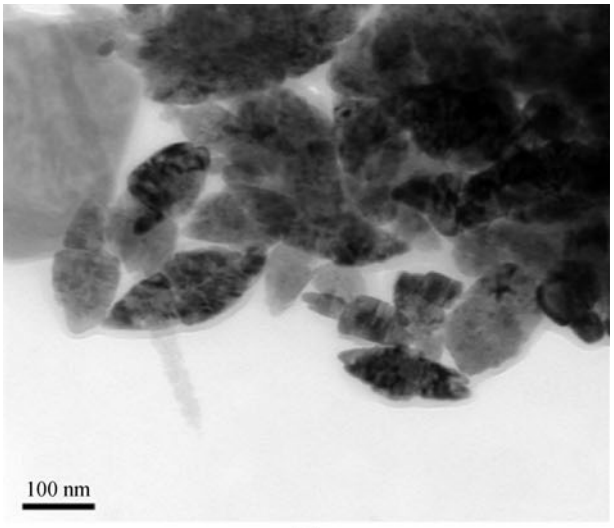

(a)

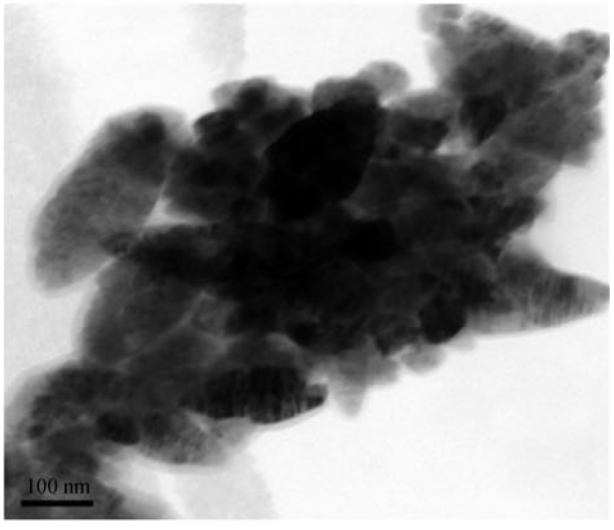

(b)

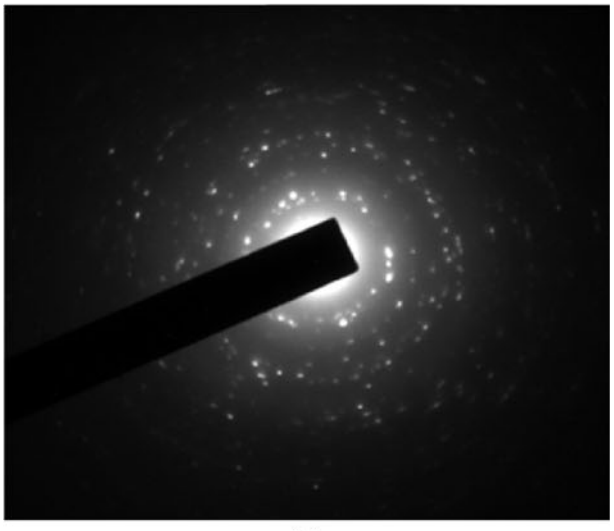

(c)

Fig. 9 (a) and (b) TEM images of bipods grown on glass substrate; (c) selected area electron diffraction (SAED) pattern of bipods

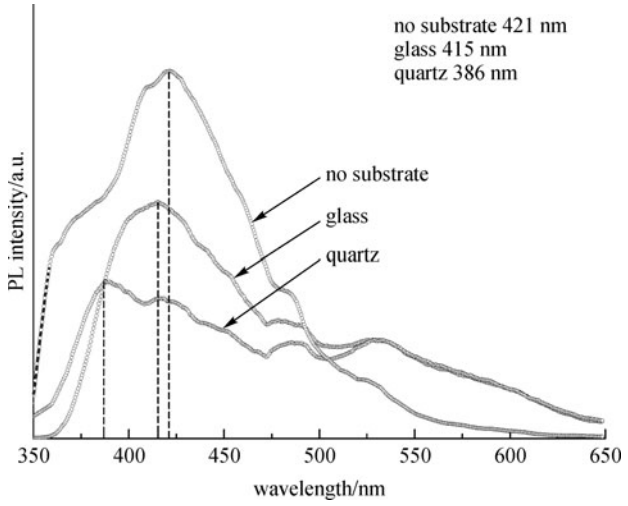

Fig. 10 Room temperature PL of ZnO monopods and bipods grown on glass and quartz

volume ratio for nanocrystals, large numbers of defects are created at the interface of substrates and thin film. The various defect energy levels have been calculated by Sun using full potential linear muffin tin orbital method [23]. The various defect energy levels of ZnO nanocrystals are shown in Fig. 11. The defect related emissions are much more pronounced in chemically grown ZnO nanocrystals. The PL spectrum of ZnO monopods, grown without any substrate, show strong violet emission peaks around 425 nm due to carrier recombination between zinc interstitial and hole in the valance band [4,23]. This violet emission is also accompanied by few weaker blue and green emission peaks at 486 and 530 nm respectively. The emission peak at 486 nm originates due to positively charged zinc vacancy (V_{Zn^+}). The green emission is the result of the existence of singly ionised oxygen vacancy [23]. The PL spectrum of the ZnO bipods, grown on glass and quartz substrates, also show similar PL emission peaks (for glass: 415, 484, and 530 nm; for quartz: 418, 486, and 530 nm) except a prominent UV peak at 386 nm in case of quartz substrates. The PL peak around 386 nm for the ZnO film deposited on the quartz substrate can be related to the excitonic recombination in ZnO [24,25]. The exciton

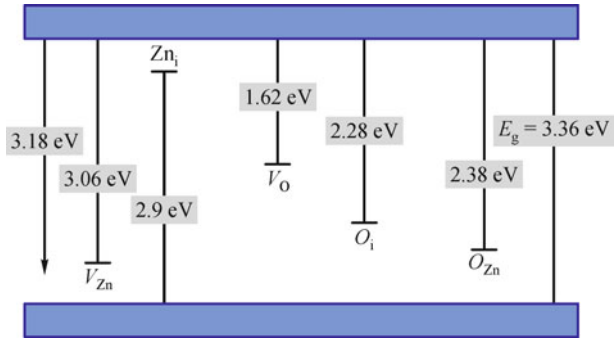

Fig. 11 Eenergy levels of various defect states of ZnO [23]

binding energy of ZnO is about 60 meV. Room temperature thermal energy may be sufficient to make free the bound exciton as the excitonic binding energy being few meV only. Thus exciton may be observed at room temperature. In our case the excitonic level emission around 386 nm for the ZnO film on quartz substrate is very close to that reported value of 380 nm excitonic recombination for Si substrate [13] corresponding to the free exciton. However, in case of glass substrate no UV emission peak was observed. This is because of the amorphous nature of glass that leads to the creation of more defects in the thin film resulting the strong defect related visible emission compared to the band edge UV emission. A small shift by 2–3 nm of the PL peak at 486 nm is observed as compared to the substrate free growth which is due to the strain at the interface of the thin film and substrates (lattice mismatch). The various PL emission peaks from various substrates and their origins are listed in Table 2. However these need further investigations.

Table 2 Various PL emission peaks and their origins

	no substrate	glass	quartz	origin of emission
PL emission peaks	–	–	386	band edge emission
	421	415	418	recombination bet Zn_i and hole in VB
	486	484	486	zinc vacancy (V_{Zn^+})
	530	530	530	singly ionised oxygen vacancy

4 Conclusions

In conclusion, we have fabricated transparent ZnO thin film grown over various substrates. The thin film is composed of bipods-like crystals. But in absence of any substrate, the morphology of the material looks like monopods. The thin film grown on quartz substrate shows a strong UV-PL at 386 nm owing to the excitonic recombination in the ZnO. This emission is accompanied by some defect related emissions. The defect related emission is almost similar for ZnO thin film grown on glass substrate. The small shift of various visible PL peaks is the result of strain arising at the thin film and substrate interface which is different for different substrate. Thus our investigation results will be very useful in understanding the substrate effect on the morphology and PL emission from thin film nanostructured materials.

References

1. Wong E M, Searson P C. ZnO quantum particle thin films fabricated by electrophoretic deposition. Applied Physics Letters, 1999, 74

(20): 2939–2941
2. Vanheusden K, Seager C H, Warren W L, Tallant D R, Voigt J A. Correlation between photoluminescence and oxygen vacancies in ZnO phosphors. Applied Physics Letters, 1996, 68(3): 403–405
3. Wang H Q, Wang G Z, Jia L C, Tang C J, Li G H. Polychromatic visible photoluminescence in porous ZnO nanotubes. Journal of Physics D: Applied Physics, 2007, 40(21): 6549–6553
4. Samanta P K, Patra S K, Roy C P. Violet emission from flower-like bundle of ZnO nanosheets. Physica E: Low-Dimensional Systems and Nanostructures, 2009, 41(4): 664–667
5. Ma J N, Ji F, Zhang D, Ma H, Li S. Optical and electronic properties of transparent conducting ZnO and ZnO:Al lms prepared by evaporating method. Thin Solid Films, 1999, 357: 98–101
6. Baxter J B, Schmuttenmaer C A. Conductivity of ZnO nanowires, nanoparticles, and thin films using time-resolved terahertz spectroscopy. Journal of Physical Chemistry B, 2006, 110(50): 25229–25239
7. Kong X Y, Wang Z L. Spontaneous polarization-induced nanohelixes, nanosprings, and nanorings of piezoelectric nanobelts. Nano Letters, 2003, 3(12): 1625–1631
8. Nakamura Y. Solution-growth of Zinc oxide nanowires for dye-sensitized solar cells. MATERIALS · NNIN REU, Research Accomplishments, 2006, 74–75
9. Huang M H, Mao S, Feick H, Yan H, Wu Y, Kind H, Weber E, Russo R, Yang P. Room-temperature ultraviolet nanowire nanolasers. Science, 2001, 292(5523): 1897–1899
10. Lin B X, Fua Z X, Jia Y B. Green luminescent center in undoped zinc oxide films deposited on silicon substrates. Applied Physics Letters, 2001, 79(7): 943–945
11. Lee M K, Tu H F. Ultraviolet emission blueshift of ZnO related to Zn. Journal of Applied Physics, 2007, 101(12): 126103
12. Liu M, Kitai A H, Mascher P. Point defects and luminescence centres in zinc oxide and zinc oxide doped with manganese. Journal of Luminescence, 1992, 54(1): 35–42
13. Teng X M, Fan H T, Pan S S, Ye C, Li G H. Photoluminescence of ZnO thin films on Si substrate with and without ITO buffer layer. Journal of Physics D: Applied Physics, 2006, 39(3): 471–476
14. Wu J J, Liu S C. Low-temperature growth of well-aligned ZnO nanorods by chemical vapor deposition. Advanced Materials, 2002, 14(3): 215–218
15. Hu H, Huang X, Deng C, Chen X, Qian Y. Hydrothermal synthesis of ZnO nanowires and nanobelts on a large scale. Materials Chemistry and Physics, 2007, 106(1): 58–62
16. Zhu Y W, Zhang H Z, Sun X C, Feng S Q, Xu J, Zhao Q, Xiang B, Wang R M, Yu D P. Efficient field emission from ZnO nanoneedle arrays. Applied Physics Letters, 2003, 83(1): 144–147
17. Samanta P K, Basak S, Roy C P. Electrochemical growth of ZnO microspheres and nanosheets. Advanced Science Letters, 2011, 4 (2): 554–557
18. Fouchet A, Prellier W, Mercey B, Méchin L, Kulkarni V N, Venkatesan T. Investigation of laser-ablated ZnO thin films grown with Zn metal target: a structural study. Journal of Applied Physics, 2004, 96(6): 3228–3233
19. Mondal S P, Das K, Dhar A, Ray S K. Characteristics of CdS nanowires grown in a porous alumina template using a two-cell method. Nanotechnology, 2007, 18(9): 095606
20. Samanta P K, Patra S K, Chaudhuri P R. Visible emission from ZnO nanorods synthesized by a simple wet chemical method. International Journal of Nanoscience and Nanotechnology, 2009, 1(1–2): 81–90
21. Sugunan A, Warad H C, Boman M, Dutta J. Zinc oxide nanowires in chemical bath on seeded substrates: role of hexamine. Journal of Sol-Gel Science and Technology, 2006, 39(1): 49–56
22. Hu X L, Zhu Y J, Wang S W. Sonochemical and microwave-assisted synthesis of linked single-crystalline ZnO rods. Materials Chemistry and Physics, 2004, 88(2–3): 421–426
23. Xu P S, Sun Y M, Shi C S, Xu F Q, Pan H B. The electronic structure and spec-tral properties of ZnO and its defects. Nuclear Instruments and Methods in Physics Research Section B, 2003, 199: 286–290
24. Wu J J, Liu S C. Low-temperature growth of well-aligned ZnO nanorods by chemical vapor deposition. Advanced Materials, 2002, 14(3): 215–218
25. Zeng H, Li Z, Cai W, Liu P. Strong localization effect in temperature dependence of violet-blue emission from ZnO nanoshells. Journal of Applied Physics, 2007, 102(10): 104307